# Ultrasonic study on complex glass system doped with erbium oxide

Ahmed M. Eid[a)]
*Ultrasonic Department, National Institute of Standards, Giza, Egypt*

Mohamed A. Farag, Khaled Abd-ullah Abd El-Rahman, and Mohamed M. El-Okr
*Physics Department, Faculty of Science, El-Azhar University, Cairo, Egypt*

(Received 25 August 2015; accepted 14 January 2016)

Glasses doped with rare earth elements (lanthanide series) are the most popular materials used in upconversion devices. The main aspect to develop these devices is to find suitable host materials for rare earth ions. The host material should have a high transmission of the upconverted photons, high thermal stability, good mechanical properties, low price, and easy to manufacture and shaping. Present work is concerned with studying the mechanical and structural properties for the oxide glass system doped with rare earth metal (erbium oxide, $Er_2O_3$). Ultrasonic pulse-echo technique is used to measure the sound velocities in the glass system ($30\%B_2O_3{\cdot}30\%Bi_2O_3{\cdot}20\%Li_2O{\cdot}10\%BaO{\cdot}10\%Pb_3O_4{\cdot}xEr_2O_3$), ($x$ = 0, 0.5, 1, 2, 3, 4) mol%. Ultrasound velocities (longitudinal and shear) are measured as a function of the $Er_2O_3$ content at a frequency of 4 MHz for longitudinal wave and 2 MHz for the shear wave at a temperature of 300 K. The elastic moduli and some physical parameters, such as Debye temperature, coordination number, and compressibility, were evaluated. Furthermore, the dimensionality of the glass network has been calculated in terms of the $d$ ratio which equals $G/B$ ratio. These parameters beside the x-ray diffraction, differential scanning calorimetry, and Fourier Transform Infrared (FTIR) measurements throw more light on the structure of the glass system. The measurements in this study exhibit remarkable anomalous changes in the network structure of the investigated glass doped with $Er_2O_3$.

## I. INTRODUCTION

Rare earth, as active ions, doped materials have been investigated as upconversion media for several years, but it is still holding a great challenging to find a suitable host material to be applied onto the photovoltaic (PV) device. Glass materials are preferred as a host material due to their stability and the capability of easy shaping for these PV devices into slips, lenses, and all other optical shapes.

Upconversion is difficult to generate in conventional oxide glasses due to their high phonon energies, corresponding to the stretching vibrations of the oxide glass's network former. However, oxide glasses have attractive properties, such as high chemical stability and ease of fabrication. Many oxide glasses have been studied intensively to find the suitable upconversion host material. The prepared glass with the molar composition (mol%) $30B_2O_3$–$30Bi_2O_3$–$20Li_2O$–$10BaO$–$10Pb_3O_4$ (B30·Bi30·Li20·Ba10·Pb10) is considered a stable glass with a wide range of transparency (450–2500 nm), high density (6.3 g/cm$^3$). The long infrared cutoff edge indicated that the phonon energy of (B30·Bi30·Li20·Ba10·Pb10) glass is small compared to other conventional oxide glasses. This work is concerned with studying the physical properties of B30·Bi30·Li20·Ba10·Pb10 glass doped with rare earth, erbium ions.

Heavy metal oxide glasses (HMOs) like $Pb_2O_3$ and $Bi_2O_3$ doped with rare earth oxides (REOs) attract the researchers due to their significant technological applications. These glasses play an important role in the development of many optoelectronic devices such as lasers, sensors, hole burning high-density memories, and optical fibers.[1–4] The HMOs can exist in the glass as a network modifier and as a network former depending on the type of bond between the cation and various counterpart oxides. In addition, lead–bismuth or lead borate glasses have been tested as matrix materials for developing new optical devices, and adding trivalent rare earth ions affects the local structure of the glass network. REO and HMO form new bonds with the surrounding ligands in the glass network that causes a variation in the structure of borate network ligands. The structure of borate glasses is not only a random distribution of $BO_3$ triangle and $BO_4$ tetrahedral, but also an aggregation of different concentrations of these units to form well defined and stable groups, such as diborate, triborate, tetraborate, etc., which constitute the random three-dimensional network.[5–7] Aset et al.[8] studied the temperature dependences of the adiabatic elastic stiffness's $C_{11}$ and $C_{44}$ and related elastic properties in rare earth metaphosphate glasses. Sampaio et al. measured the

Contributing Editor: Himanshu Jain
[a)]Address all correspondence to this author.
e-mail: ameid11@yahoo.com
DOI: 10.1557/jmr.2016.27

 © Materials Research Society 2016 

https://doi.org/10.1557/jmr.2016.27 Published online by Cambridge University Press

elastic moduli for calcium aluminosilicate glasses with <10 mol% of $SiO_2$ doped with $Er_2O_3$ and $Yb_2O_3$ and concluded that the addition of small amounts (<1.5 mol%) of $Er_2O_3$ or $Yb_2O_3$ may have induced a decrease <5% in the elastic modulus, consistent with the hypothesis that the rare earth ions act as network modifiers, disrupting the glass lattice.[9] Earlier, Kumar et al. investigated the elastic moduli and other parameters using ultrasound $LiF–B_2O_3$ glasses doped with certain rare earth ions.[10] Honma et al.[11] examined electronic oxide polarizability of $Bi_2O_3·B_2O_3$ glasses and clarified that Bi–O bonds are largely ionic. They discovered new nonlinear optical crystalline phase $[x_1RE_2O_3–x_2BiO_3–(1 - x)BO_3]$ in the crystallized glasses of $RE_2O_3–Bi_2O_3–B_2O_3$ (RE: La, Gd, Sm). Thermal and optical properties of glasses $Bi_2O_3·B_2O_3$ systems were studied by Becker[12] and Ehrt.[13] In addition, the optically transparent crystallized glasses $Bi_2O_3·B_2O_3$ containing rare earth ions or nanoregions of ferroelectric crystals have received much interest, because such materials have a potential for laser host, tunable waveguide and tunable fiber grating.[14] The elastic moduli are important parameters which are used in fiber drawing, and it was reported with a view to drawing 20 $Bi_2O_3·80B_2O_3·1RE_2O_3$ in mol% (where, RE = Pr, Nd, Sm, Eu, Gd, and Er) as a waveguide optical glass. It has been pointed out that the structure of alkali borate glasses is strongly dependent upon the species of alkali ion. Infrared and Raman studies on alkali borate glasses by many researchers[15–18] have also shown that the ratio $N_4$ decreases and the number of nonbridging oxygens (NBOs) increases as the glass content is changed from Li to Cs with the same amount, and different kinds of borate groups are formed. Kodama et al.[7,19] studied the anomalous behavior of ultrasonic velocity in cesium borate and rubidium borate glasses, they assumed these composite glasses to be composed of three structural units, and that the elastic property of these glasses has been analyzed in terms of the three structural units, $N_4$ has been calculated as a function of composition to calculate the change in the amount of each structural unit that causes the anomalous behavior of ultrasonic behavior.

Many researchers studied the dimensional parameters of the glass network, the $d$ ratio and the conformable ratio ($G/C_{12}$) and the constants of elasticity in different types of glasses[4,20–24] were investigated and it was found that these parameters are in a correlation with the constant of elasticity of the glass.

Generally, the ultrasonic technique is one of the best methods to determine the constants of elasticity of such kinds of glasses and to compare these values with previous studies.[25–31] Therefore, the goal of this paper is to complete the study that has been performed on the elastic properties of these glasses. From these studies, we can extract valuable information about the structure of the prepared glasses. Information about the structure of these glasses can be deduced after calculation of the elastic moduli, Debye temperature, Poisson's ratio, cross-link density, and the fractal bond connectivity.

## II. EXPERIMENTAL PROCEDURES

Glass system of composition $30B_2O_3–30Bi_2O_3–20Li_2O–10BaO–10Pb_3O_4–xEr_2O_3$ ($x$-mol%) has been prepared by conventional melting and quenching method, where $x = 0$, 0.5, 1, 2, 3, and 4. The starting material is reagent grade $H_3BO_3$, $(BiO)_2CO_3$, $Li_2CO_3$, $BaCO_3$, and $Pb_2O_3$.

About 25 g of the starting raw materials, with purity 99.99%, were preheated at 200–300 °C to get rid of undesired gasses, then the powder was mated at 950–1000 °C for 20–25 min in a porcelain crucible in the electric furnace in the air atmosphere. The melts were shaken during preparation to ensure homogeneity. The melt was poured into preheated molds at 250 °C. The prepared samples were subjected to annealing at 250 °C for several hours, then the furnace was left to cool to room temperature.

After preparation, the two opposite sides of the samples were polished to be suitable for the ultrasonic velocity measurements. The deviation in the parallelism of the two opposite side faces was about ±8 μm.

### A. Glass characterization

X-ray diffraction (XRD) patterns of the prepared samples were recorded with a Philips x-ray diffractometer (Eindhoven, The Netherlands) using monochromatized Cu $K_{\alpha 1}$ radiation of wave length 1.54056 Å from a fixed source operated at 45 kV and 9 mA.

To determine the glass transition temperature of the prepared glass, differential scanning calorimetry (DSC) was used. The measurements were performed by thermal analyzer SDT Q600 V20.9 Build 20 (TA Instruments, New Castle, Delaware) in the temperature range 25–600 °C with heating rate 10 °C/min in a nitrogen atmosphere.

To study the structure units of the prepared samples, the FTIR absorption spectra were recorded by Jasco FTIR (Jasco Corporation, Tokyo, Japan) in the range 400–4000 $cm^{-1}$ with a resolution of 1 $cm^{-1}$ using the KBr pellet technique. The infrared spectra were corrected for the dark current noises and normalized to eliminate the concentration effect of the powder sample in the KBr disc.

The density (ρ) of the glass samples was measured by applying the Archimedes principle at 25 °C using toluene of density 0.868 $g/cm^3$ as an immersion liquid and applying the relation:

$$\rho = \rho_b \left( \frac{W_a}{W_a - W_b} \right) \quad , \qquad (1)$$

where, $\rho_b$ is the density of the toluene, $W_a$ and $W_b$ are the sample weights in the air and the toluene, respectively.

https://doi.org/10.1557/jmr.2016.27 Published online by Cambridge University Press

The molar volume ($V_m$) has been calculated as $M/\rho$, and $M$ is the molecular mass of the samples.

The ultrasonic wave velocities longitudinal ($U_l$) and shear ($U_s$) at room temperature were measured using the pulse-echo method. In this method, x-cut transducer operated at fundamental frequency 4 and 2 MHz y-cut transducer (Krautkramer, Hurth, Germany) and a digital ultrasonic flaw detector (Krautkramer USIP 60) were used. The uncertainty in the measurement of the ultrasonic velocity is $\pm 9.5$ ms$^{-1}$ for longitudinal wave velocity and $\pm 3$ ms$^{-1}$ for shear wave velocity. The two velocities besides the density were utilized in determining two independent second-order elastic constants. The ultrasonic velocities and the density were used to determine the elastic moduli and Debye temperature ($\theta_D$) of the glass system. The uncertainty in the elastic moduli $\pm 0.12$ GPa and $\pm 0.006$ for Poisson's ratio ($\sigma$).

The constants of elasticity such as longitudinal ($L$), shear ($G$), bulk ($B$), and the ($C_{12}$) modulus can be determined from the relations[32,33];

$$L = C_{11} = \rho U_l^2 \quad , \tag{2}$$

$$G = C_{44} = \rho U_s^2 \quad , \tag{3}$$

$$B = \left(L - \left(\frac{4}{3}\right)G\right) \quad , \tag{4}$$

$$C_{12} = (C_{11} - 2C_{44}) = (L - 2G) \quad . \tag{5}$$

Poisson's ratio ($\sigma$) is reported to provide more information about the character of the bonding forces than any of the other elastic coefficients.[34,35] Poisson's ratio ($\sigma$) is related to Young's modulus ($E$) and shear modulus ($G$) by the equation:

$$\sigma = \left(\frac{L - 2G}{2(L - G)}\right) = \frac{E}{2G} - 1 \quad , \tag{6}$$

$$\sigma = \frac{\left(U_l^2 - 2U_s^2\right)}{2\left(U_l^2 - U_s^2\right)} \quad , \tag{7}$$

$$E = \frac{3\rho U_s^2\left[U_l^2 - \left(\frac{3}{4}\right)U_s^2\right]}{\left(U_l^2 - U_s^2\right)} \quad . \tag{8}$$

## III. RESULTS AND DISCUSSION

### A. X-ray studies

The XRD patterns of 3 sample powders ($Er_0$, $Er_1$, and $Er_4$ mol%) depicted in Fig. 1 were found to show no discrete sharp peaks, but broad halo at around 26–30°, which reflected the amorphous nature of the prepared samples. This indicates the absence of long-range atomic arrangement and the periodicity of the three-dimensional network in the glassy materials. To confirm the glassy state of the prepared samples, DSC measurements were performed as shown in Fig. 2. The characteristic thermal temperatures such as the glass transition temperature, $T_g$, the onset crystallization temperature $T_c$, and the full crystallization peak $T_p$ were selected on the DSC curves to confirm the amorphous nature of the samples.

### B. Infrared spectra

Infrared spectroscopy is usually used to obtain essential information concerning the arrangement of the structural units of the studied glasses. It is assumed that vibrations of structural units of the glass network are

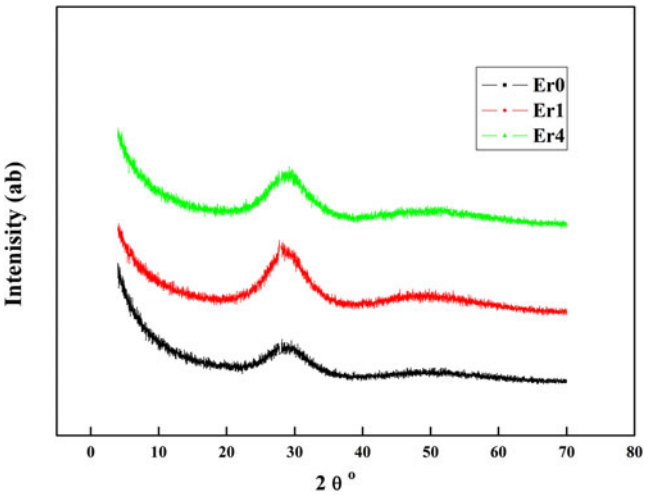



FIG. 1. The XRD pattern of the prepared glasses doped with $Er_2O_3$ (0, 1, and 4 mol%).

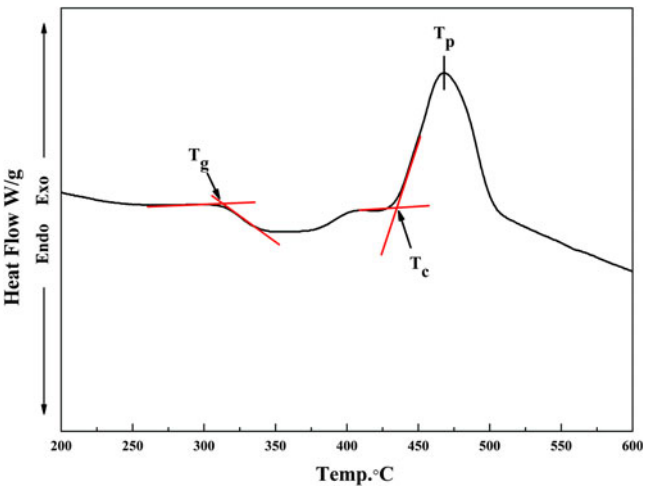



FIG. 2. $T_g$, $T_c$, and $T_p$ locations on DSC curve of the blank glass sample.

https://doi.org/10.1557/jmr.2016.27 Published online by Cambridge University Press

independent of vibration of other neighboring units.[36] Also, it is well known that vitreous $B_2O_3$ consists of $BO_3$ units, which can be associated to form six-membered boroxol rings. Therefore, the obtained FTIR data of the prepared glasses in the range 400–1600 $cm^{-1}$ are shown in Fig. 3. To investigate the role of the glass modifier such as $Er_2O_3$ on the active peaks in the measured spectra, a deconvolution process should be taking place using Gaussian fitting. The deconvolution of the measured spectra is shown in Table I. The active peaks of the blank sample were found to be at 432, 556, 712, 736, 838, 909, 990, 1116, 1168, 1233, and 1291 $cm^{-1}$.

It is known from previous work that the vibrational modes of borate glasses can be coordinated as follows:

(i) The band observed at 432–556 $cm^{-1}$ is attributed to the vibration of Bi–O–Bi in the [$BiO_6$] octahedron.[6,37,38]

(ii) 712–736 $cm^{-1}$ originates due to the bending vibration of B–O–B in [$BO_3$] triangles.[39,40]

(iii). Vibration band at 838 $cm^{-1}$ (Ref. 41) in [$BiO_3$] polyhedral.

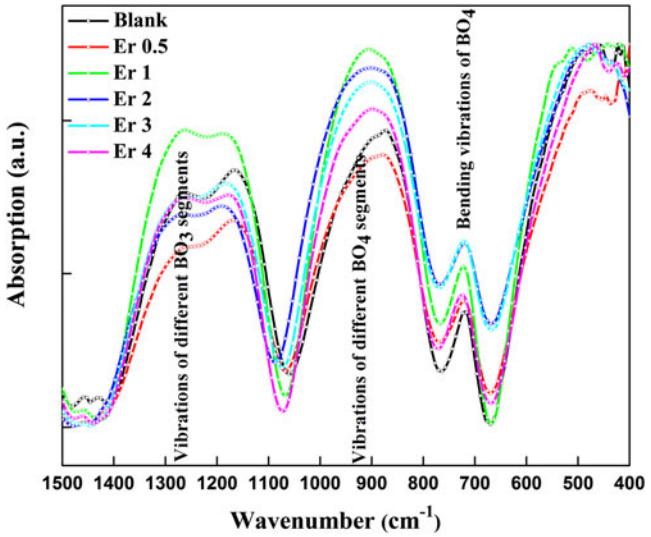



FIG. 3. FTIR spectra of (B30·Bi30·Li20·Ba10·Pb10) glass doped with $Er_2O_3$ content.

TABLE I. The vibration modes of the studied glasses doped with $Er_2O_3$.

| Blank ($Er_0$) | $Er_{0.5}$ | $Er_1$ | $Er_2$ | $Er_3$ | $Er_4$ |
|---|---|---|---|---|---|
| 432 | 378 | 429 | 425 | 403 | 439 |
| 556 | 529 | 562 | 555 | 545 | 564 |
| 712 | 711 | 710 | 711 | 712 | 711 |
| 736 | 738 | 736 | 743 | 741 | 737 |
| 838 | 853 | 858 | 853 | 850 | 866 |
| 909 | 949 | 951 | 950 | 943 | 960 |
| 990 | 1016 | 1010 | 1023 | 1013 | 1015 |
| 1116 | 1115 | 1123 | 1130 | 1124 | 1124 |
| 1168 | 1164 | 1173 | 1177 | 1177 | 1166 |
| 1233 | 1234 | 1269 | 1264 | 1276 | 1253 |
| 1291 | 1307 | 1345 | 1344 | 1351 | 1336 |

(iv) 909–990, 1116, and 1168 $cm^{-1}$ are attributed to the stretching vibration of B–O–B in [$BO_4$] triangles.[42,43]

(v) 1233–1291 $cm^{-1}$ is attributed to the stretching vibration of the B–O–B in [$BO_3$] tetrahedron.[44,45]

It can be noted from Table I and Fig. 3, that further addition of $Er_2O_3$ to the blank sample alters the band position and intensity. The addition of $Er_2O_3$, to $B_2O_3$ network, causes a conversion of $BO_3$ into $BO_4$ units. The relation between $BO_4$ and $BO_3$ is usually determined by $N_4$ which is given by the relation[46]:

$$N_4 = \frac{A_4}{A_4 + A_3} \quad , \tag{9}$$

where $A_4$ presents the relative area under the peak of vibrational modes ranging between 800 and 1200 $cm^{-1}$ for borate and $A_3$ is the relative area under the peak of the vibrational modes in the range 600–800 and 1200–1600 $cm^{-1}$. The $N_4$ diagram is shown in Fig. 4. The studied glass system is a complex one and contains various structural units, such as $B_4$(Er), $B_3$(Er), $B_4$(Pb), $PbO_4$, and $BO_3$. These units are, respectively, $BO_4$ units modified by $Er_2O_3$, $BO_3$ units modified by $Er_2O_3$, $BO_4$ units modified by PbO, network former $PbO_4$ units, and symmetric $BO_3$ units. The $N_4$ values can be used to trace the change in concentration of these structural units as a function of the $Er_2O_3$ content.[47–50] It can be noted from Table I that the addition of $Er_2O_3$ to the blank sample alters the band position and intensity. This addition causes a nonuniform behavior of the compositional dependence of $N_4$ on $Er_2O_3$. Now, to investigate the role of $Er_2O_3$, the concentration of the various structural units should be computed as follows.

The concentration, (mol%), of $B_2O_3$ in the form of $BO_4$ units, can be given as

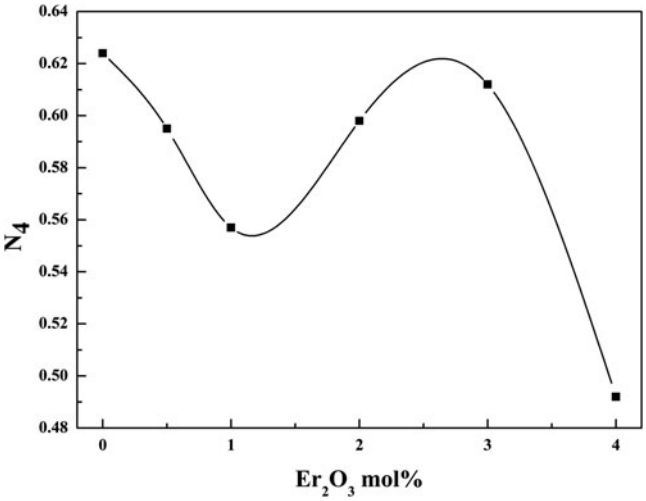



FIG. 4. The coordination number $N_4$ of the glass samples as a function of $Er_2O_3$ content.

https://doi.org/10.1557/jmr.2016.27 Published online by Cambridge University Press

$$C_{BO_4} = N_4 C_{B_2O_3} \quad ,$$

where $C_{B_2O_3}$ represents the concentration (mol%) of $B_2O_3$. The quantity, $C_{BO_3}$ (mol%), of symmetric $BO_3$ units, is then

$$C_{BO_3} = (1 - N_4) C_{B_2O_3} \quad .$$

Since $Er_2O_3$ is considered as network modifier, then the concentration, $C_{B_4(Er)}$ (mol%), of $B_2O_3$ that forms $B_4$(Er) units would be

$$C_{B_4} = 3x \quad ,$$

where $x$ is the concentration of $Er_2O_3$, and the concentration, $C_{B_4(Pb)}$, of $B_2O_3$ that forms $B_4$(Pb) unit is

$$C_{B_4(Pb)} = C_{BO_4} - C_{B_4(Er)} \quad .$$

It might be clear that $C_{B_4(Pb)}$ equals to the concentration of the modifier $Pb_2O_3$. It follows that the concentration, $C_{PbO_4}$, of PbO that forms $PbO_4$ units can be expressed as

$$C_{PbO_4} = C_{PbO} - C_{B_4(Pb)} \quad .$$

Table II lists the variations of the concentration of the various structural units against $Er_2O_3$. It is shown that there is a decrease in $C_{B_4(Pb)}$ and an increase in $C_{B_4(Er)}$ and $C_{B_3(Pb)}$ with increasing $Er_2O_3$ content. Also, it is clear that the concentration of $B_4$(Pb) is going to vanish at $Er_2O_3$ content >4 mol%. The decrease in the concentration of $B_4$(Pb) units is accompanied by an increase in the concentration of $C_{B_4(Er)}$ and $C_{B_3(Er)}$ units. Moreover, by using the data presented in Table II and the molar volume values ($V_m$), the overall concentration ($n_u$) of the structural units in glass (total number of structural units/cm$^3$)[50] can be calculated as a function of the $Er_2O_3$ concentration according to the relation;

$$n_u = 6.0022 \times 10^{23} \left( C_{BO_3} + C_{B_4(Er)} + C_{B_4(Pb)} + C_{PbO_4} \right) / V_m \quad .$$

Now, Fig. 4 reveals that the addition of $Er_2O_3$ into the glass network will decrease the $N_4$ value from 0 to 1 mol% of $Er_2O_3$ while from 1 to 3 mol% increase the $N_4$ value which is followed by a decrease beyond this concentration. The behavior of $N_4$ obeys the behavior of the concentration of $BO_4$ structural units. This behavior is confirmed from the decrease of the concentration of the structural units of the HMOs and the increase of the concentration of the structural units of $Er_2O_3$.[47] This indicates the modifier role of $Er_2O_3$ in the glass network, i.e., it affects the probability of $BO_4$ formation by breaking up tetrahedral bonds of $BO_4$ units and introducing coordination defects known as dangling bonds.[48,49] Figure 5 and Table II shows a minimum of $n_u$ at 2 mol% $Er_2O_3$.

### C. Density and molar volume studies

Density in the glassy state depends on the chemical composition of the samples. Then it is important to characterize the structure of the glass (compactness and/or softening), the coordination number, the change in geometrical configuration, and bond density, etc. In general, when metal oxides are added to the glass network, the density may be decreased or increased with increasing the ratios of the oxides without any anomalous behavior. However, in the studied glass system, there is an anomalous behavior. Figure 6 and Table III shows the variation of the density and the molar volume behavior by increasing the $Er_2O_3$ content.

Inspection of Table III and Fig. 6 reveals that the density of the blank glass sample, (0 mol% $Er_2O_3$), was 6287.29 kg/m$^3$, and by adding the $Er_2O_3$ to the glass, the density decreased with no remarkable values to be 6138 kg/m$^3$ at 0.5 mol% $Er_2O_3$ content and 6138.60 kg/m$^3$ at 1 mol% $Er_2O_3$. Beyond this concentration of $Er_2O_3$, density drops to a lower value reaching 5950.72 kg/m$^3$ for the 2 mol% $Er_2O_3$ content sample. This may be explained by adding $Er_2O_3$ to the glass system that will increase the open structure and the NBOs in the glass network which increases the overall volume and hence decreasing the density. In the range $2 \leq Er_2O_3 \leq 4$ (mol %), the density increases remarkably again by increasing the $Er_2O_3$ content in the samples from 6150.62 to 6165.43 kg/m$^3$. In this range, $Er_2O_3$ starts to enter the glass network by reducing the NBOs and increasing the compactness of the glass and more of bridging oxygens (BOs) will be created leading to increasing the rigidity of

TABLE II. Change in concentration of various structural units as a function of the $Er_2O_3$ content.

| Sample code | $C_{BO_4}$ | $C_{BO_3}$ | $C_{B_4(Er)}$ | $C_{B_3(Er)}$ | $C_{B_4(Pb)}$ | $C_{PbO_4}$ | $n_b \times 10^{-28}$ (m$^{-3}$) | $n_u \times 10^{-28}$ (m$^{-3}$) |
|---|---|---|---|---|---|---|---|---|
| $Er_0$ | 18.72 | 11.28 | 0 | 0 | 18.72 | ... | 8.31 | 8.76 |
| $Er_{0.5}$ | 17.85 | 12.15 | 0.015 | 0.012 | 16.35 | ... | 8.05 | 8.06 |
| $Er_1$ | 16.71 | 13.29 | 0.030 | 0.024 | 13.71 | ... | 7.99 | 7.33 |
| $Er_2$ | 17.94 | 12.06 | 0.060 | 0.048 | 11.94 | ... | 7.63 | 6.38 |
| $Er_3$ | 18.36 | 11.64 | 0.090 | 0.072 | 09.36 | 0.64 | 7.77 | 6.93 |
| $Er_4$ | 14.76 | 15.24 | 0.120 | 0.100 | 02.76 | 7.24 | 7.66 | 7.27 |

https://doi.org/10.1557/jmr.2016.27 Published online by Cambridge University Press

the glass. The results are in a great agreement with the results of the infrared (IR).

The molar volume showed an opposite behavior to the density behavior with the increasing $Er_2O_3$ content. The increase in $V_m$ with increasing $Er_2O_3$ content up to 2 mol% $Er_2O_3$ may be related to the increase of $BO_3$ units. Moreover, according to Wells,[51] $Er^{3+}$ ion is coordinated with seven oxygen atoms, which may participate in the expansion of the studied glass network and increase the molar volume. It might be taken into consideration that one $Er_2O_3$ molecule produces six $B_4$(Er) units at the expense of $B_4$(Pb) units, which is responsible for the decrease in the number of network bonds per unit volume ($n_b$) up to 2 mol% $Er_2O_3$ as shown in Fig. 7 and Table III. The calculations of $n_b$ as a function of the $Er_2O_3$ concentration according to the relation;

$$n_b = \frac{N_A n_f}{V_m} \left(m^{-3}\right) \quad ,$$

where, $N_A$ is the Avogadro's number, and $n_f$ is the number of network bonds per unit formula.

The decrease in $V_m$ at 3 mol% $Er_2O_3$ content can be attributed to the increase in the concentration of [$BO_4$] units and $n_b$ which reduces the formation of NBOs.

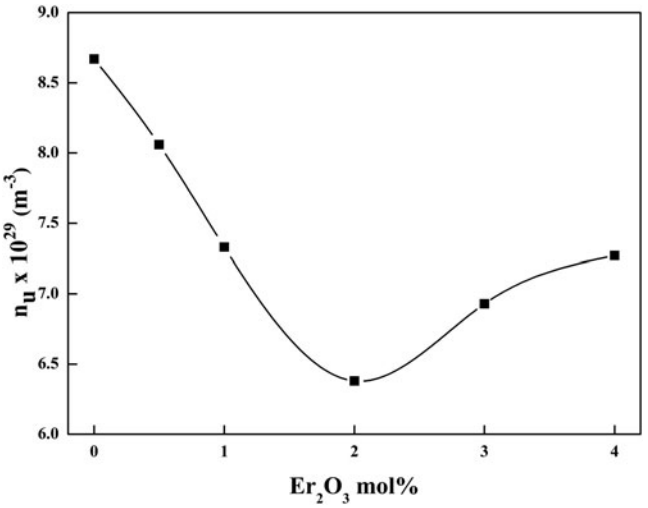



FIG. 5. Dependence of the structural unit concentrations ($n_u$) on $Er_2O_3$ content.

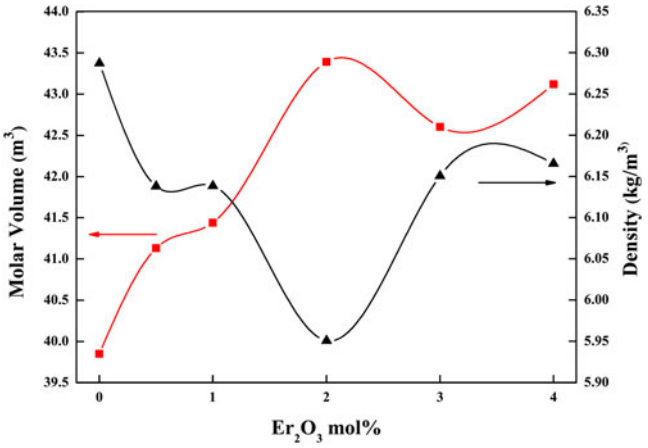



FIG. 6. Variation of density and molar volume of the prepared glass with increasing $Er_2O_3$ content.

TABLE III. Density (ρ), molar volume ($V_m$), and ultrasonic velocity longitudinal ($U_l$) and shear ($U_s$).

| Sample code | ρ (kg/$m^3$) | $V_m \times 10^5$ ($m^3$) | $U_l$ (m/s) | $U_s$ (m/s) |
|---|---|---|---|---|
| $Er_0$ | 6287.29 | 3.99 | 3573.12 | 2178.31 |
| $Er_{0.5}$ | 6138.00 | 4.11 | 3851.55 | 2368.72 |
| $Er_1$ | 6138.60 | 4.14 | 3888.89 | 2153.85 |
| $Er_2$ | 5950.72 | 4.34 | 3770.12 | 1892.34 |
| $Er_3$ | 6150.62 | 4.26 | 3929.58 | 2227.55 |
| $Er_4$ | 6165.43 | 4.31 | 4011.07 | 2137.07 |

## D. Ultrasonic and elastic moduli studies

Ultrasonic velocity is very sensitive to the variation of the glass network structure. The experimental ultrasonic velocity data in the glass system are given in Table III and Figs. 8(a) and 8(b). It is inferred from the table and figures that there is an initial increase in velocity up to 0.5 mol% of $Er_2O_3$ for the transverse wave and at 1 mol% for the longitudinal force. Both of velocities decreased to reach the minimum at 2 mol% $Er_2O_3$ content with a higher rate for the shear velocity. Further addition of $Er_2O_3$ causes an increase in the velocities again for up to 4 mol% $Er_2O_3$. This can be attributed to the sensitivity of the glass system for the shear stress more than the compression stress.

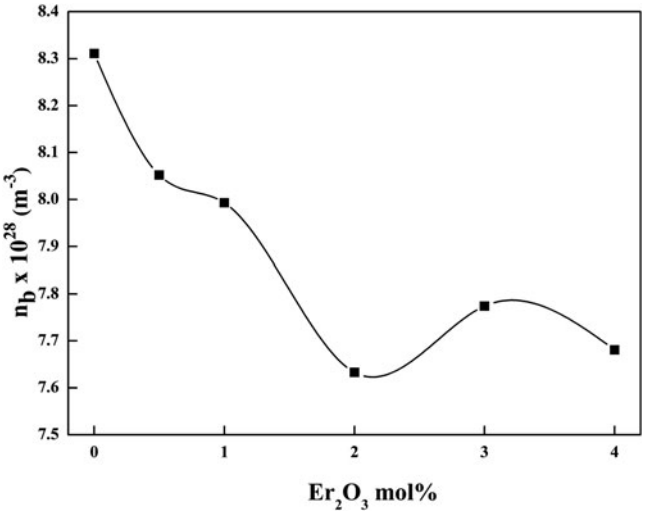



FIG. 7. Dependence of the number of network bonds per unit volume ($n_b$) on $Er_2O_3$ content.

https://doi.org/10.1557/jmr.2016.27 Published online by Cambridge University Press

Elastic properties of materials are usually characterized by Young's modulus, shear modulus, bulk modulus, and Poisson's ratio. For isotropic materials only two of these elastic constants are independent and other constants are calculated by using the relations given by the theory of elasticity. The best choice for these two independent moduli is considered as the shear modulus and the bulk modulus. The shear modulus, ($G$), relates to strain response of a body to shear or torsional stress. It involves a change of shape without change of volume. On the other hand, the bulk modulus, ($B$), describes the strain response of a body to hydrostatic stress involving a change in volume without change of shape.

The composition dependence of the elastic moduli showed an initial increase in longitudinal modulus ($L$), shear modulus ($G$), Young's modulus ($E$) and the dimensionality parameters ($d$) and ($G/C_{12}$), Table IV and Figs. 9(a) and 9(b), up to 0.5 mol% of $Er_2O_3$. Beyond this limit, there is a decrease in these parameters to reach a minimum value with 2 mol% of $Er_2O_3$ then to start to increase again at 3 mol% of the $Er_2O_3$ content. At 4 mol% of $Er_2O_3$ content, most of the elastic moduli decrease then few slight increases. In the studied glass system, maybe there is a modification of $BO_4$ structural units by $Er_2O_3$ by forming $B_4$(Er) and $B_3$(Er) units. As the $Er_2O_3$ content increases, the concentration of $B_4$(Er) and $B_3$(Er) units increases at the expense of the units of HMOs. The increase of $B_4$(Er) and $B_3$(Er) units expands the structure, therefore, the changes in the type and concentration of these structural units produce a minimum in the compositional dependence of the constants of elasticity with $Er_2O_3$ around 2 mol% $Er_2O_3$. The two ratios, $d$ and $G/C_{12}$, describing the dimensionality of the structure of the studied glasses have an inversion around 2 mol% $Er_2O_3$ in a good correlation with the behavior of the constants of elasticity as shown in Table IV and Figs. 8 and 9.

Figure 10 shows the compositional dependence of the bulk modulus ($B$) against the $Er_2O_3$ content. The behavior of the bulk modulus ($B$) behaves in a different way to that of the other elastic moduli $L$, $G$, and $E$. This abnormal behavior may be due to the fact that the rate of change in the shear stress is greater than that of the compression stress according to the equation.[4]

The differential relationships of σ with $E$ and $G$, and $U_l$ and $U_s$ can be obtained by differentiating Eqs. (6) and (7), respectively. The differential forms of the above equations are:

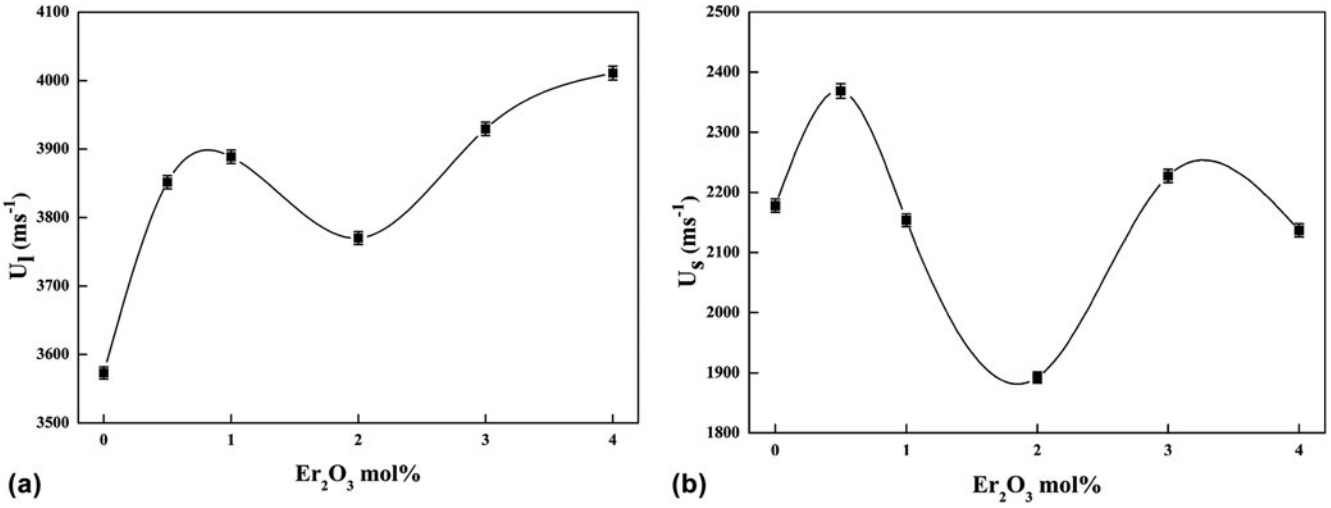



FIG. 8. Ultrasonic velocities (a) longitudinal $U_l$ and (b) shear $U_s$ with $Er_2O_3$ content.

TABLE IV. The mean velocity ($U_m$), longitudinal modulus ($L$), shear modulus ($G$), bulk modulus ($B$), Young's modulus ($E$), the microhardness ($H$), ratio ($G/C_{12}$), $E/G$ ratio, $d$ ratio and Poisson's ratio (σ) of all glass samples.

| Sample code | $U_m$ (m/s) | $L$ (GPa) | $G$ (GPa) | $B$ (GPa) | $E$ (GPa) | $H$ (GPa) | $G/C_{12}$ | $E/G$ | $d$ ratio | σ |
|---|---|---|---|---|---|---|---|---|---|---|
| $Er_0$ | 2405.92 | 80.27 | 29.83 | 40.49 | 71.85 | 5.88 | 1.448 | 2.409 | 2.946 | 0.204 |
| $Er_{0.5}$ | 2614.07 | 91.05 | 34.44 | 45.13 | 82.37 | 6.98 | 1.553 | 2.392 | 3.052 | 0.196 |
| $Er_1$ | 2399.44 | 92.84 | 28.48 | 54.87 | 72.83 | 4.20 | 0.794 | 2.558 | 2.076 | 0.279 |
| $Er_2$ | 2122.37 | 84.58 | 21.31 | 56.17 | 56.75 | 2.39 | 0.508 | 2.663 | 1.517 | 0.334 |
| $Er_3$ | 2476.88 | 94.98 | 30.52 | 54.28 | 77.11 | 4.82 | 0.899 | 2.527 | 2.249 | 0.263 |
| $Er_4$ | 2387.60 | 99.19 | 28.16 | 61.65 | 73.31 | 3.72 | 0.657 | 2.604 | 1.827 | 0.302 |

https://doi.org/10.1557/jmr.2016.27 Published online by Cambridge University Press

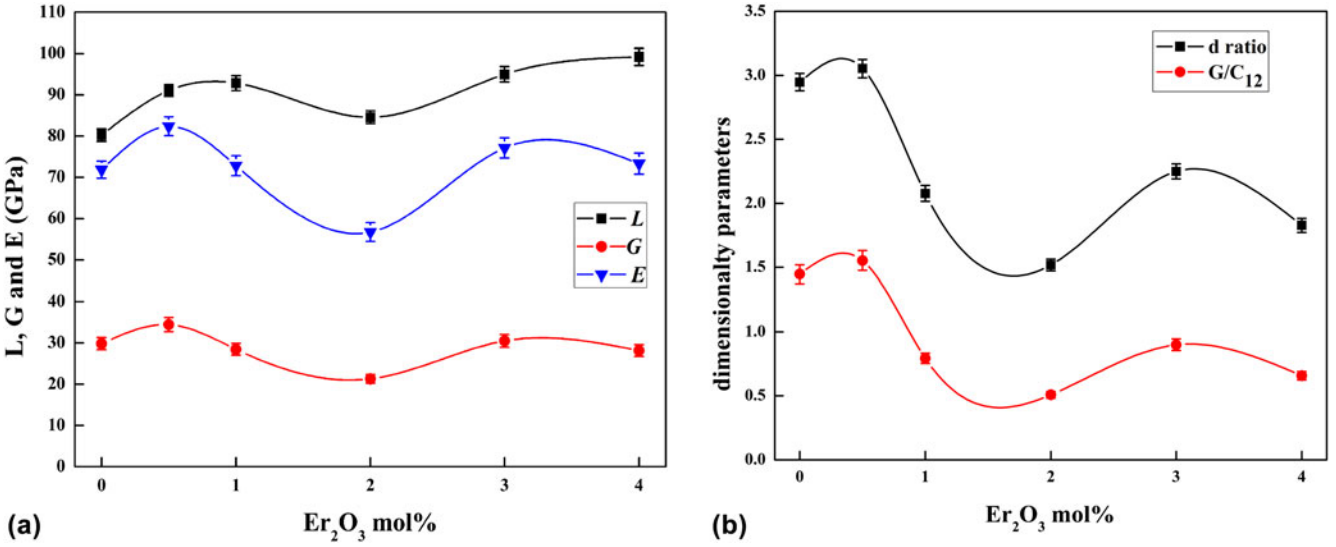



FIG. 9. Elastic constants (a) $L$, $G$, and $E$ (b) the dimensionality parameters with the $Er_2O_3$ content.

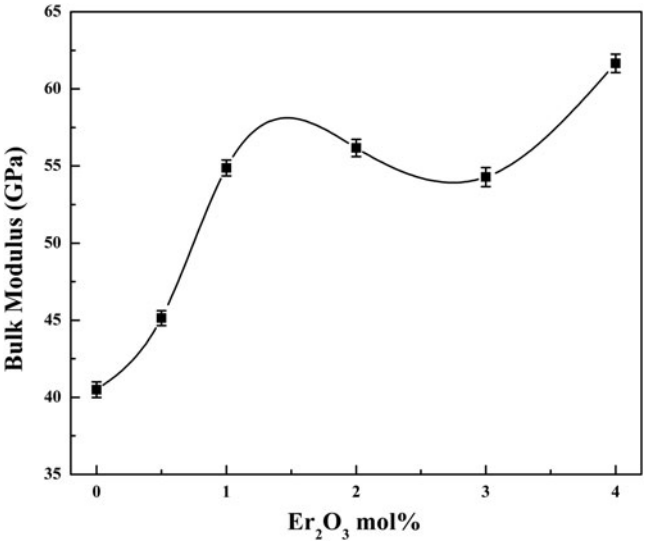



FIG. 10. Composition dependence of the bulk modulus $B$ of the studied glasses.

$$\frac{d\sigma}{\sigma} = \frac{1}{1-(2G/E)}\left(\frac{dE}{E} - \frac{dG}{G}\right) \quad , \qquad (10)$$

$$\frac{d\sigma}{\sigma} = \frac{\left(U_l^2 - U_s^2\right)}{\left(U_l^2 - U_s^2\right)\left(U_l^2 - 2U_s^2\right)}\left(\frac{dU_l}{U_l} - \frac{dU_s}{U_s}\right) \quad . \qquad (11)$$

Variation of Poisson's ratio ($\sigma$) depends on the variation of the values and relative values of $E$ and $G$ in Eq. (10) and $U_l$ and $U_s$ in Eq. (11). For any material $E$ and $G$ as well as $U_l$ and $U_s$ tend to increase or decrease together. Therefore, we cannot decide that the variation of $\sigma$ in the same or opposite direction to that of $E$ and $G$. Using Eqs. (10) and (11), we can predict the behavior of $\sigma$ according to which of the two elastic constants varies more than the other. If Eqs. (10) and (11) are positive, then $\sigma$ varies in the same direction of $E$ or $U_l$, and $G$ or $U_s$ and vice versa. However, for isotropic solids, $\sigma$ is bounded practically by 0 and 1/2.

A high crosslink density material has a Poisson's ratio in the order of 0.1–0.2 while low crosslink density materials have Poisson's ratio between 0.3 and 0.5.[52,53] Accordingly, Poisson's ratio of the investigated glass is about 0.2 at 0 and 0.5 mol% $Er_2O_3$ content, while it increased to 0.33 at 2 mol% $Er_2O_3$ content, Fig. 11.

Microhardness expresses the required stress to eliminate the free volume (deformation of the network) of the glass. The microhardness ($H$) was calculated from Young's modulus ($E$) and Poisson's ratio ($\sigma$) according to the relationship:

$$H = \frac{E(1-2\sigma)}{6(1+\sigma)} \quad . \qquad (12)$$

The increase in the microhardness indicates the increase in the rigidity of the glass. The microhardness as shown in Fig. 12 decreases as Poisson's ratio increases and vice versa. However, for isotropic solids, $\sigma$ is bounded practically by 0 and 0.5.

Dimensionality of the amorphous structure can be described with two important parameters related to the elasticity's constants,[54,55] one of them is called the $d$ ratio which equals to 4 $G/B$. In the three-dimensional tetrahedral coordination polyhedron such as $SiO_2$, the value of the $d$ ratio is 3 and in the two-dimensional layer structures, it equals 2. The second important parameter is the ratio $G/C_{12}$,[55] which is considered as an indicator of the character of the force field. This parameter equals to 1 in the case of the central force type; otherwise, the force

https://doi.org/10.1557/jmr.2016.27 Published online by Cambridge University Press

is not central. On the other hand, the $G/C_{12}$ ratio approaches unity as the central force field may reduce the fraction of the broken bonds in the network structure of the glass.[54] Another parameter is the ratio between Young's modulus and shear modulus $E/G$. The results indicated 2-dimensional network with noncentral force.

The Debye temperature ($\theta_D$) is an important parameter of solids; it represents the temperature at which nearly all the vibration modes are excited. The softening temperature ($T_S$) is another important parameter defined as the temperature at which viscous flow changes to plastic flow. The two temperatures can be calculated according to the relations;

$$\theta_D = \left(\frac{h}{K_B}\right)\left(\frac{3nN_A}{4\pi V_m}\right)^{1/3} U_m \quad , \tag{13}$$

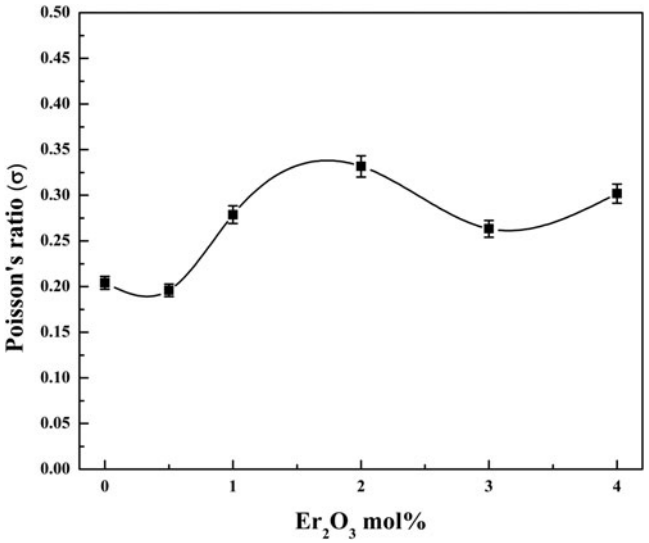



FIG. 11. Relation between Poisson's ratio (σ) of the glass and $Er_2O_3$ content.

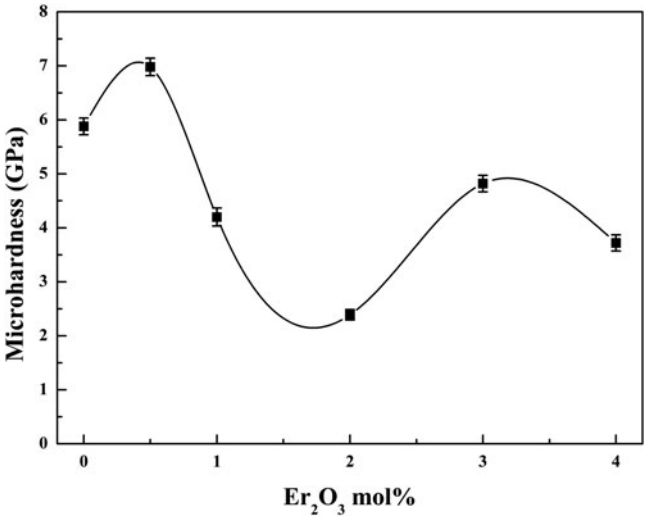



FIG. 12. Variation of microhardness $H$ with increasing $Er_2O_3$ content.

where, $h$ is Plank's constant, $K_B$ is Boltzmann's constant, $N_A$ is Avogadro's number, $V_m$ is the molar volume, $n$ is the number of atoms in the chemical formula, and $U_m$ is the mean ultrasonic velocity.

$$U_m = \left(\frac{1}{3}\left(\frac{1}{{U_L}^3} + \frac{2}{{U_S}^3}\right)\right)^{-\frac{1}{3}} \quad . \tag{14}$$

The softening temperature can be evaluated from the relation

$$T_S = \left(\frac{M_w}{c\rho}\right){U_S}^2 \quad , \tag{15}$$

where $M_w$ is the molecular mass and $c$ is constant equals [$0.5074 \times 10^5$ cm/($K^{-1/2}$ s)].[56]

Debye temperature ($\theta_D$) and the softening temperature ($T_S$) are illustrated in Table V and Fig. 13. It can be observed that both the Debye and softening temperatures increased from 292.37 and 372 K to 314.91 and 454.9 K, respectively, as the content of $Er_2O_3$ was increased to be 0.5 mol%. The increase in the mean ultrasonic velocity

TABLE V. The softening temperature ($T_s$) and the Debye temperature ($\theta_D$).

| Sample code | $T_s$ (K) | $\theta_D$ (K) |
|---|---|---|
| $Er_0$ | 372.7 | 292.37 |
| $Er_{0.5}$ | 454.9 | 314.91 |
| $Er_1$ | 378.9 | 288.87 |
| $Er_2$ | 306.1 | 252.54 |
| $Er_3$ | 416.7 | 297.61 |
| $Er_4$ | 388.2 | 286.74 |

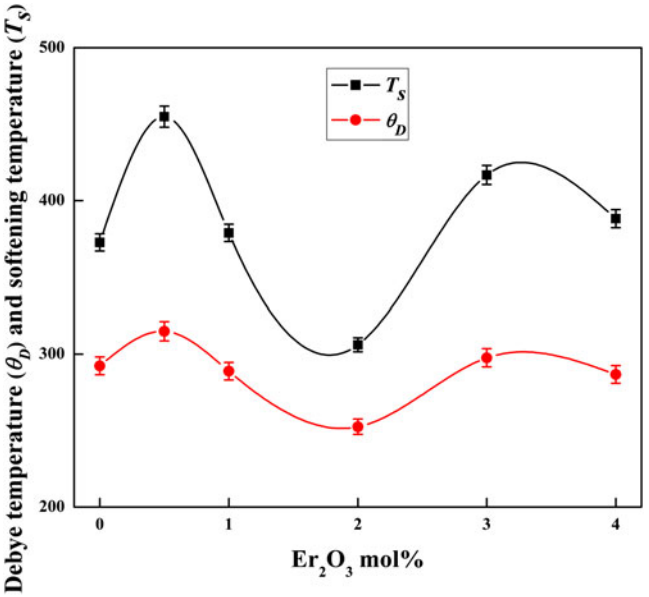



FIG. 13. Variation of the ($\theta_D$) and ($T_s$) with $Er_2O_3$ content.

https://doi.org/10.1557/jmr.2016.27 Published online by Cambridge University Press

($U_m$) and consequently the increase in Debye and softening temperatures are mainly due to the decrease of the number of NBOs as a direct effect of the insertion of $Er_2O_3$ ions, with 0.5% concentration, into the glass network structure. By increasing the Er content up to 2% creates NBOs and causes loose packing in the glass structure and a reduction in the vibrations of the lattice, slight increase in $n_u$ and NBOs at 3 and 4% $Er_2O_3$ concentration. The two temperatures followed the behavior of the ultrasonic velocities.

## IV. CONCLUSION

The density, infrared bands, and the ultrasonic velocity in the complex glass system doped with $Er_2O_3$ plotted against composition are found to exhibit anomalous behavior with increasing mol% of $Er_2O_3$. It also shows a maximum and minimum and another maximum depending on the amount of the NBOs. Also, the values of the elastic moduli exhibit the same behavior.

## REFERENCES


1. A. Mekki, Kh. A. Ziq, D. Holland, and C.F. McConville: Magnetic properties of praseodymium ions in $Na_2O$–$Pr_2O_3$–$SiO_2$ glasses. *J. Magn. Magn. Mater.* **260**, 60 (2003).
2. Y. Kuisheng, X. Huili, W. Rinang, K. Jiaqiang, W. Wiezhong, Z. Bin, and Z. Xiyan: Research on up—conversion mechanism in $Er^{3+}$/$Yb^{3+}$ co-doped oxyfluoride glass. *J. Rare Earths* **24**, 175 (2006).
3. J. Pisarska, W. Pisarski, and W. Ryba-Romanowski: Laser spectroscopy of $Nd^{3+}$ and $Dy^{3+}$ ions in Lead borate glasses. *Opt. Laser Technol.* **42**(5), 805 (2010).
4. Y. Saddeek: Structural, and acoustical studies of lead sodium borate glasses. *J. Alloys Compd.* **467**(1–2), 14 (2009).
5. V. Lavin, P. Babu, C. Jayasankar, I.R. Martin, and V.D. Rodriguez: On the local structure of $Eu^{3+}$ ions in oxyfluoride glasses: Comparison with fluoride and oxide glasses. *J. Chem. Phys.* **115**, 10935 (2001).
6. H. Doweidar and Y. Saddeek: FTIR and ultrasonic investigations on modified bismuth borate glasses. *J. Non-Cryst. Solids* **355**, 348 (2009).
7. M. Kodama: Anomalous behavior of ultrasonic velocity in rubidium borate glasses. *J. Am. Ceram. Soc.* **74**, 2603 (1991).
8. M. Acet, T. Brennan, M. Cankurtaran, G.A. Saunders, and H. Zähres: Elastic and nonlinear acoustic properties and thermal expansion of rare-earth metaphosphate glasses. *Philos. Mag. B* **77** (6), 1633 (1998).
9. J.A. Sampaio, M.L. Baesso, S. Gama, A.A. Coelho, J.A. Eiras, and I.A. Santos: Rare earth doping effect on the elastic moduli of low silica calcium aluminosilicate glasses. *J. Non-Cryst. Solids* **304**, 193 (2002).
10. A.R. Kumar and N. Veeraiah: Acoustic investigations on LiF–$B_2O_3$ glasses doped with certain rare-earth ions. *J. Mater. Sci. Lett.* **18**, 475 (1999).
11. T. Honma, Y. Benino, T. Fujiwara, R. Sato, and T. Komatsu: New optical nonlinear crystallized glasses and YAG laser-induced crystalline dot formation in rare-earth bismuth borate system. *Opt. Mater.* **20**(1), 27 (2002).
12. P. Becker: Thermal and optical properties of glasses of the system $Bi_2O_3$–$B_2O_3$. *Cryst. Res. Technol.* **38**(1), 74 (2003).
13. D. Ehrt: Structure, properties and applications of borate glasses. *Glass Technol.* **41**(6), 182 (2000).
14. R. Ihara, T. Honma, Y. Benino, T. Fujiwara, and T. Komatsu: Second order optical nonlinearities of metastable $BiBO_3$ phases in crystallized glasses. *Opt. Mater.* **27**, 403 (2004).
15. E.I. Kamitsos, M.A. Karakassides, and G.D. Chryssikos: Cation-network interactions in binary alkali metal borate glasses. A far-infrared study. *J. Phys. Chem.* **91**, 5807 (1987).
16. E.I. Kamitsos, M.A. Karakassides, and G.D. Chryssikos: Structure of borate glasses. Part 1: Raman study of cesium, rubidium and potassium borate glasses. *Phys. Chem. Glasses* **30**(6), 229 (1989).
17. G.D. Chryssikos, E.I. Kamitsos, and M.A. Karakassides: Structure of borate glasses. Part 2. Alkali induced network modifications in terms of structure and properties. *Phys. Chem. Glasses* **31**(3), 109 (1990).
18. J. Krogh-Moe: Interpretation of the infra-red spectra of boron oxide and alkali borate glasses. *Phys. Chem. Glasses* **6**(2), 46 (1965).
19. M. Kodama, T. Hirashima, and T. Matsushita: Anomalous behavior of ultrasonic velocity in cesium borate glasses. *Phys. Chem. Glasses* **34**(4), 129 (1993).
20. A. El-Adawy and Y. Moustafa: Elastic properties of bismuth borate glasses. *J. Phys. D: Appl. Phys.* **32**(21), 2791 (1999).
21. Y. Saddeek: Structural analysis of alkali borate glasses. *Phys. B (Amsterdam, Neth.)* **344**(1–4), 163 (2004).
22. Y. Saddeek and L. Abd El Latif: Effect of $TeO_2$ on the constants of elasticity of sodium borate glasses. *Phys. B (Amsterdam, Neth.)* **348**(1–4), 475 (2004).
23. Y. Saddeek: Elastic properties of $Gd^{3+}$ doped tellurovanadate glasses using pulse-echo technique. *Mater. Chem. Phys.* **91**(1), 146 (2005).
24. R.A.H. El-Mallawany: *Tellurite Glasses Handbook: Physical Properties and Data* (CRC Press, New York, 2002).
25. A. Makishima and J. Mackenzie: Direct calculation of the Young's modulus of glass. *J. Non-Cryst. Solids* **12**(1), 35 (1973).
26. A. Makishima and J. Mackenzie: Calculation of bulk modulus, shear modulus, and Poisson's ratio of glass. *J. Non-Cryst. Solids* **17**(2), 147 (1975).
27. A. Makishima, Y. Tamura, and T. Sakaino: Constants of elasticity and refractive indices of aluminosilicate glasses containing $Y_2O_3$, $La_2O_3$, and $TiO_2$. *J. Am. Ceram. Soc.* **61**(5–6), 247 (1978).
28. B. Bridge, N. Patel, and D. Waters: On the elastic constants and structure of the inorganic oxide glasses. *Phys. Status Solidi A* **77** (2), 655 (1983).
29. B. Bridge and A. Higazy: Model of the compositional dependence of the constants of elasticity of polycomponent oxide glasses. *Phys. Chem. Glasses* **27**(1), 1 (1986).
30. J. Rocherulle, C. Ecolivet, M. Poulain, P. Verdier, and Y. Laurent: Elastic moduli of oxynitride glasses: Extension of Makishima and Mackenzie's theory. *J. Non-Cryst. Solids* **108**(2), 187 (1989).
31. S. Inaba, S. Fujino, and K. Morinaga: Young's modulus and compositional parameters of oxide glasses. *J. Am. Ceram. Soc.* **82** (12), 3501 (1999).
32. A.K. Varshneya: *Fundamentals of Inorganic Glasses* (Acadamic Press, New York, 1994).
33. F.A. Khalifa, Z.A. El-Hadi, F.A. Moustafa, and N.A. Hassan: Density and molar volume of some sodium silicate, lead borate and lead silicate glasses. *Indian J. Pure Appl. Phys.* **27**(6), 279 (1989).
34. L. Gao, S. Xue, L. Zhang, Z. Sheng, F. Ji, W.S. Dai, L. Yu, and G. Zeng: Effect of alloying elements on properties and microstructures of SnAgCu solders. *Microelectron. Eng.* **87**(11), 2025–2034 (2010).
35. S.K. Seo, S.K. Kang, D.Y. Shih, and H.M. Lee: The evolution of microstructure and microhardness of Sn–Ag and Sn–Cu solders during high temperature aging. *Microelectron. Reliab.* **49**, 288 (2009).


https://doi.org/10.1557/jmr.2016.27 Published online by Cambridge University Press

36. F.H. ElBatal, S.Y. Marzouk, N. Nada, and S.M. Desouky: Gamma-ray interaction with copper-doped bismuth–borate glasses. *Phys. B* **391**, 88 (2007).
37. I. Ardelean, S. Cor, R.C. Lucacel, and O. Hulpus: EPR and FT-IR spectroscopic studies of $B_2O_3$–$Bi_2O_3$–MnO glasses. *Solid State Sci.* **7**, 1438 (2005).
38. Y. Dimitriev and V. Mihailova: Infrared spectral investigation of bismuthate glasses. In: *Proceedings of the 16th International Congress on Glass*, Vol. **3**; Fernandez Navarro and Jose Maria, eds. (Boletín de la Sociedad Española de Cerámica y Vidrio, Madrid, 1992); pp. 293–298.
39. R. Iordanova, V. Dimitrov, Y. Dimitriev, and D. Klissurski: Glass-formation and structure of glasses IN the $V_2O_5$–$MoO_3$–$Bi_2O_3$ system. *J. Non-Cryst. Solids* **180**, 58 (1994).
40. A. Manisha Pal, K. Hirota, Y. Tsujigami, and H. Sakata: Structural and electrical properties of $MoO_3$-$TeO_2$ glasses. *J. Phys. D: Appl. Phys.* **34**, 459 (2001).
41. V. Dimitrov, Y. Dimitrov, and A. Montenero: IR spectra and structure of $V_2O_5$–$GeO_2$–$Bi_2O_3$ glasses. *J. Non-Cryst. Solids* **180**, 51 (1994).
42. S. Sindhu, S. Sanghi, A. Agarwal, V.P. Seth, and N. Kishore: Structural, optical, physical and electrical properties of $V_2O_5$.SrO. $B_2O_3$ glasses. *Spectrochim. Acta, A* **64**, 196 (2006).
43. A. Kashif and A. Abd El-Maboud, and A. Ratep: Effect of $Nd_2O_3$ addition on structure and characterization of lead bismuth borate glass. *Results Phys.* **4**, 1 (2014).
44. A.H. Verhoef and H.W. Den Hartog: Infrared spectroscopy of network and cation dynamics in binary and mixed alkali borate glasses. *J. Non-Cryst. Solids* **182**, 221 (1995).
45. E.I. Kamitsos, A.P. Patsis, M.A. Karakassides, and G.D. Chryssikos: Infrared reflectance spectra of lithium borate glasses. *J. Non-Cryst. Solids* **126**, 52 (1990).
46. K. El-Egili: Infrared studies of $Na_2O$–$B_2O_3$–$SiO_2$ and $Al_2O_3$–$Na_2O$–$B_2O_3$–$SiO_2$ glasses. *Phys. B* **325**, 340 (2003).
47. Y. Zhou, S. Dai, J. Wang, T. Xu, Q. Nie, and S. Huang: Spectroscopic properties of $Er^{3+}$:$^4I_{13/2}$ level in $Bi_2O_3$–$B_2O_3$–$GeO_2$–$Na_2O$ glasses. *J. Alloys Compd.* **472**, 203 (2009).
48. D. Maniu, I. Ardelean, T. Iliescu, S. Cinta, and O. Cozar: Raman spectroscopic investigations of the oxide glass system $(1 - x)(3B_2O_3{\cdot}K_2O)$ xMO (MO = $V_2O_5$ or CuO). *J. Mol. Struct.* **410/411**, 291–294 (1997).
49. M. Krishna Murthy, K.S.N. Murthy, and N. Veeraiah: Dielectric properties of NaF $B_2O_3$ glasses doped with certain transition metal ions. *Bull. Mater. Sci.* **23**(4), 285 (2000).
50. H. Doweidar and Y.B. Saddeek: Effect of $La_2O_3$ on the structure of lead borate glasses. *J. Non-Cryst. Solids* **356**, 1452 (2010).
51. A. Wells: *Structural Inorganic Chemistry*, 4th ed. (Clarendon Press, Oxford, 1975).
52. R. El-Mallawany: Structural interpretations on tellurite glasses. *Mater. Chem. Phys.* **63**, 109 (2000).
53. V. Rajendran, N. Palanivelu, D.K. Modak, and B. K. Chaudhuri: Ultrasonic investigation on ferroelectric $BaTiO_3$ doped $80V_2O_5$–20PbO oxide glasses. *Phys. Status Solidi A* **180**, 467 (2000).
54. L. Hwa, K. Hsieh, and L. Liu: Constants of elasticity of low silica calcium alumino–silicate glasses. *Mater. Chem. Phys.* **78**(1), 105 (2003).
55. C. Chen, Y. Wu, and G. Hwa: Temperature dependence of elastic properties of ZBLAN glasses. *Mater. Chem. Phys.* **65**(3), 306 (2000).
56. R. El-Mallawany, N. El-Khoshkhany, and H. Afifi: Ultrasonic studies of $(TeO_2)50$–$(V_2O_5)50$–x$(TiO_2)$ glasses. *Mater. Chem. Phys.* **95**, 321 (2006).


https://doi.org/10.1557/jmr.2016.27 Published online by Cambridge University Press